OPEN ACCESS

University of BRISTOL

Publisher's PDF, also known as Version of record

Link to published version (if available):
10.1371/journal.pone.0144309

Link to publication record in Explore Bristol Research
PDF-document

This is the final published version of the article (version of record). It first appeared online via Public Library of Science at http://journals.plos.org/plosone/article?id=10.1371/journal.pone.0144309. Please refer to any applicable terms of use of the publisher.

University of Bristol - Explore Bristol Research
General rights

Cellular Hypertrophy and Increased Susceptibility to Spontaneous Calcium-Release of Rat Left Atrial Myocytes Due to Elevated Afterload

Haifei Zhang[1], Mark B. Cannell[1], Shang Jin Kim[1¤], Judy J. Watson[1], Ruth Norman[2], Sarah C. Calaghan[2], Clive H. Orchard[1], Andrew F. James[1]*

1 Cardiovascular Research Laboratories, School of Physiology, Pharmacology & Neuroscience, University of Bristol, Bristol, BS8 1TD, United Kingdom, 2 School of Biomedical Sciences, Garstang, University of Leeds, Leeds, LS2 9JT, United Kingdom

¤ Current address: Department of Pharmacology and Toxicology, College of Veterinary Medicine, Chonbuk National University, 664–14 Deockjin-Dong, Jeonju-City, South Korea, 561–756
* a.james@bristol.ac.uk

Abstract

Atrial remodeling due to elevated arterial pressure predisposes the heart to atrial fibrillation (AF). Although abnormal sarcoplasmic reticulum (SR) function has been associated with AF, there is little information on the effects of elevated afterload on atrial Ca^{2+}-handling. We investigated the effects of ascending aortic banding (AoB) on Ca^{2+}-handling in rat isolated atrial myocytes in comparison to age-matched sham-operated animals (Sham). Myocytes were either labelled for ryanodine receptor (RyR) or loaded with fluo-3-AM and imaged by confocal microscopy. AoB myocytes were hypertrophied in comparison to Sham controls (P<0.0001). RyR labeling was localized to the z-lines and to the cell edge. There were no differences between AoB and Sham in the intensity or pattern of RyR-staining. In both AoB and Sham, electrical stimulation evoked robust SR Ca^{2+}-release at the cell edge whereas Ca^{2+} transients at the cell center were much smaller. Western blotting showed a decreased L-type Ca channel expression but no significant changes in RyR or RyR phosphorylation or in expression of Na^+/Ca^{2+} exchanger, SR Ca^{2+} ATPase or phospholamban. Mathematical modeling indicated that $[Ca^{2+}]_i$ transients at the cell center were accounted for by simple centripetal diffusion of Ca^{2+} released at the cell edge. In contrast, caffeine (10 mM) induced Ca^{2+} release was uniform across the cell. The caffeine-induced transient was smaller in AoB than in Sham, suggesting a reduced SR Ca^{2+}-load in hypertrophied cells. There were no significant differences between AoB and Sham cells in the rate of Ca^{2+} extrusion during recovery of electrically-stimulated or caffeine-induced transients. The incidence and frequency of spontaneous Ca^{2+}-transients following rapid-pacing (4 Hz) was greater in AoB than in Sham myocytes. In conclusion, elevated afterload causes cellular hypertrophy and remodeling of atrial SR Ca^{2+}-release.

Introduction

Atrial fibrillation (AF) is the most common sustained arrhythmia, represents a major risk factor for stroke and is associated with high morbidity and mortality[1]. The most prevalent risk factor for the development of AF is hypertension[1, 2]. Animal models have shown that hypertension and elevated afterload cause structural and cellular remodeling of the atria that establishes a substrate for re-entrant arrhythmias[3–7]. However, the trigger mechanism(s) initiating AF are less clear[1] although abnormalities in Ca^{2+} handling are likely to play an important role[8–11]. In addition, tachyarrhythmia-induced electrical remodeling in the form of reduced atrial effective refractory period (AERP)[12], linked to reduced L-type Ca^{2+} channel (LTCC) current (I_{CaL}) density and increased inward-rectifier K^+ currents[13–15] contribute to the stabilization of the arrhythmia.

Atrial myocytes from AF patients show abnormal sarcoplasmic reticulum (SR) Ca^{2+} handling and an increased rate of spontaneous diastolic Ca^{2+} release compared with myocytes from patients in sinus rhythm[9–11]. Spontaneous diastolic release of SR Ca^{2+} can cause delayed afterdepolarizations (DADs), which constitute a major mechanism underlying focal triggered activity[8]. Thus, the AF-associated remodeling of Ca^{2+} handling is consistent with an increased susceptibility to triggered activity in atria from AF patients[8, 12]. Atrial myocytes from AF patients show complex and variable patterns of intracellular Ca^{2+} transport[8], but the extent to which this is altered in afterload-induced remodeling prior to the development of AF is unknown. Propagating Ca^{2+}-induced Ca^{2+} release, which is known to be arrhythmogenic in ventricular myocytes[16], depends on the microscopic cellular architecture[17, 18] and might be altered during hypertension-induced cellular remodeling. We have examined this possibility by analyzing cell geometry, ryanodine receptor labeling and the spread of Ca^{2+} signals across cells from sham-operated and elevated afterload (aortic-banded) animals[4].

Materials and Methods

All procedures were conducted in accordance with the Animals (Scientific Procedures) Act 1986 of the United Kingdom and were approved by the Research Ethics Committee of the University of Bristol. Surgical procedures were conducted under general anaesthesia (80 mg/kg ketamine and 8 mg/kg xylazine).

Animal model with elevated afterload

A gradual increase in left ventricular afterload was achieved by partial stenosis of the ascending aorta in weanling rats, as described previously[4]. Briefly, 32 male Wistar rats (B&K Universal Ltd, UK), body weight 100–120 g (3–4 weeks of age), were subject to general anesthesia (80 mg/kg ketamine and 8 mg/kg xylazine), intubated and ventilated and a right thoracotomy performed. In 16 of these (AoB), a silk ligature (3–0) was tied around the ascending aorta to the outer diameter of a blunt 20-gauge needle (0.91 mm). The remaining 16 time-matched sham-operated controls (Sham) were subject to the same procedure except that a suture was not tied around the aorta. Experiments were conducted 20±1 weeks post-surgery.

Cell isolation and storage

Left atrial myocytes were isolated from AoB and Sham hearts by Langendorff perfusion of the heart with a collagenase-containing solution and stored in Kraftbrühe (KB) solution at ~4°C until use, as described previously[3]. Cells were stored in Kraftbrühe (KB) solution containing (in mM), 70 L-glutamic acid, 30 KCl, 10 HEPES, 1 EGTA, 5 $MgCl_2$, 5 Na-pyruvate, 20 taurine,

10 D-glucose, 5 succinic acid, 5 creatine, 2 Na_2ATP, and 5 β-hydroxybutyric acid (pH 7.2) in a refrigerator (~4°C)[19].

Confocal microscopy

Images were obtained from live and fixed cells using a laser scanning confocal microscope (LSM 510, Zeiss, Germany). The confocal aperture was set so that the confocal plane was ≤1 μm with a ×63 oil-immersion objective lens (Plan-Neofluar, numerical aperture 1.2, Zeiss, Germany).

Cell labeling

To visualize the cell membrane, left atrial myocytes were stained with 5 μM di-8-ANEPPS (Invitrogen, UK) at room temperature (RT) for 5 minutes. After removal of unloaded dye by centrifugation (400 rpm, 40 s) and re-suspension in dye-free Tyrode's solution, di-8-ANEPPS-loaded cells were transferred to a bath mounted on the LSM 510 (Zeiss, Germany). To examine the expression and localization of ryanodine receptors (RyR), myocytes were allowed to settle on poly-l-lysine coverslips for 1 h. Cells were fixed in 4% paraformaldehyde (PFA) for 10 min and subsequently permeabilized using 0.1% Triton-X for 10 min at RT. Fixed and permeabilized cells were incubated with 5 μg/ml of RyR antibody (Pierce Antibodies, MA3-916) for 1 h followed by incubation with 2 μg/ml Alexa Fluor 488-conjugated anti-mouse secondary antibody (Molecular Probes, A21121) for 1 h. Images were analyzed using ImageJ (NIH) and using routines written in IDL (Boulder, CO). The periodicity of the staining was investigated by obtaining the fluorescence profile along the longitudinal axis of the cell. The power spectrum of the fluorescence profile was calculated using the fast Fourier transform (FFT) and a Gaussian function was fitted to the first harmonic (IgorPro 3.16B, Wavemetrics Inc., OR). The spatial frequency corresponding to the peak of the power spectrum gave a measure of the periodic interval and the amplitude of the peak normalized as a percentage of the frequency-independent component of the spectrum provided a measure of the intensity of staining associated with the striations[20].

Western blotting

10 μg samples of tissue homogenates were run on 6% reducing SDS-PAGE gels and transferred onto Immobilon-P membrane. Blots were probed with anti-ryanodine receptor 2 (anti-RyR2; MA3916, Thermo Scientific, UK), S2808-specific anti-phospho-RyR2 (2808 AP, Badrilla, UK), S2814-specific anti-phospho-RyR2 (A010-31AP, Badrilla, UK), anti-α_{1c} LTCC subunit (ACC-003; Alomone, Israel), anti-SR Ca^{2+} ATPase (anti-SERCA2; MA3-919, Thermo Scientific, UK), anti-phospholamban (anti-PLB; A010-14, Badrilla, UK), S16-specific anti-phosphorylated PLB (A010-12AP, Badrilla, UK), anti-Na^+/Ca^{2+} exchanger (anti-NCX1; R3F1, Swannt, Switzerland) or anti-GAPDH (G9545; Sigma, UK) and protein bands visualized using relevant peroxidase-conjugated secondary antibodies, chemiluminescence and autoradiography. The S2808- and S2814-specific anti-phospho-RyR2 antibodies were used to investigate changes in RyR2 phosphorylation because phosphorylation at these sites for protein kinase A (PKA) and Ca^{2+}-calmodulin-dependent protein kinase II (CaMKII) has been reported to be altered in atrial fibrillation and heart failure[10, 11, 21–26]. Band density was measured using ImageJ (http://imagej.nih.gov/ij/) and normalized to GAPDH.

Ca²⁺ imaging

Atrial myocytes were re-suspended in a Tyrode's solution containing 0.75 mM Ca^{2+} and loaded with 10 μM fluo 3-AM for 6 min at 37°C. Fluo-3-AM-loaded cells were resuspended in control

Tyrode's solution containing (in mM) 134 NaCl, 4 KCl, 1.2 MgCl$_2$, 1.0 CaCl$_2$, 11 D-glucose, 10 4-(2-hydroxyethyl)-1-piperazineethanesulfonic acid (HEPES; pH 7.4) and, after 30 minutes de-esterification, transferred to a bath mounted on the stage of the LSM (Zeiss, Germany). The cells were superfused with control solution and stimulated at 0.2–1 Hz by 4-ms bi-polar supra-threshold rectangular voltage pulses via a pair platinum electrodes. Experiments were performed at room temperature. Fluo-3 was excited at 488 nm and emitted fluorescence collected at wavelengths >505 nm. SR function was examined by rapid application of the RyR agonist, caffeine (10 mM). Image analysis was performed off-line using Zeiss LSM 5 Image Examiner Software V2.81 (Zeiss, Germany) and custom routines in IDL (Boulder, CO). Linescan images of electrically-stimulated 'twitch' transients are presented as the average of >15 consecutive transients. Fluorescence was normalized to the baseline signal (F/F$_0$). Where indicated, the intracellular Ca²⁺ concentration ([Ca²⁺]$_i$) was calculated using the equation:

$$[Ca^{2+}]_i = \left(K_d \cdot \left(\frac{F}{F_0} \right) \right) / \left(\frac{K_d}{[Ca^{2+}]_{rest}} - \frac{F}{F_0} + 1 \right),$$

Eq 1

assuming a dissociation constant of fluo-3 for Ca²⁺ (K_d) of 400 nM and [Ca²⁺]$_{rest}$ = 100 nM [27], where F represents fluorescence intensity and F_0 represents the baseline F. This value for K_d was chosen to allow direct comparison of the data with a previous study of Ca²⁺ transport in rat atrial cells[28]. Ca²⁺ extrusion from the cytosol during the recovery of twitch and caffeine-induced transients were quantified by fitting the decaying phase of the transient with the equation:

$$[Ca^{2+}]_i(t) = A \cdot e^{-k.t} + c,$$

Eq 2

where t represents time, k the rate constant, A a constant representing the notional peak of the transient at $t = 0$ and c the resting level.

Modeling of diffusion

To examine the gradients of Ca²⁺ that would result from diffusive processes in cells a computer model was used to solve the general reaction-diffusion equation:

$$\frac{dX}{dt} = -D_x \cdot \nabla^2 X - \sum_B J_X + J_S,$$

Eq 3

where D_X is the diffusion coefficient for diffusible species X, J_X the reactive flux for all buffers B and J_S the source (and sinks) of Ca²⁺. Consideration of the elliptical cross-section of a cylindrical cell (see Fig 1A) suggested that the Laplacian should be solved in a two dimensional orthogonal elliptic coordinate system where symmetry allowed only one quadrant to be solved:

$$\nabla^2 X = \frac{1}{a^2 \left(cosh^2(\mu) - cos^2(v) \right)} \left(\frac{\partial^2 X}{\partial \mu^2} + \frac{\partial^2 X}{\partial v^2} \right), \ v \in \left[0, \frac{\pi}{2} \right]$$

Eq 4

related to Cartesian cell x,y coordinates by:

$$x = a \cosh(\mu) + \cos(v); \ y = a \sinh(\mu) + \sin(v)$$

Eq 5

The resulting discretization of the problem is shown in the corresponding figure. The base model major and minor axes were 10.3 and 7.6 μm respectively. Reactive fluxes were described
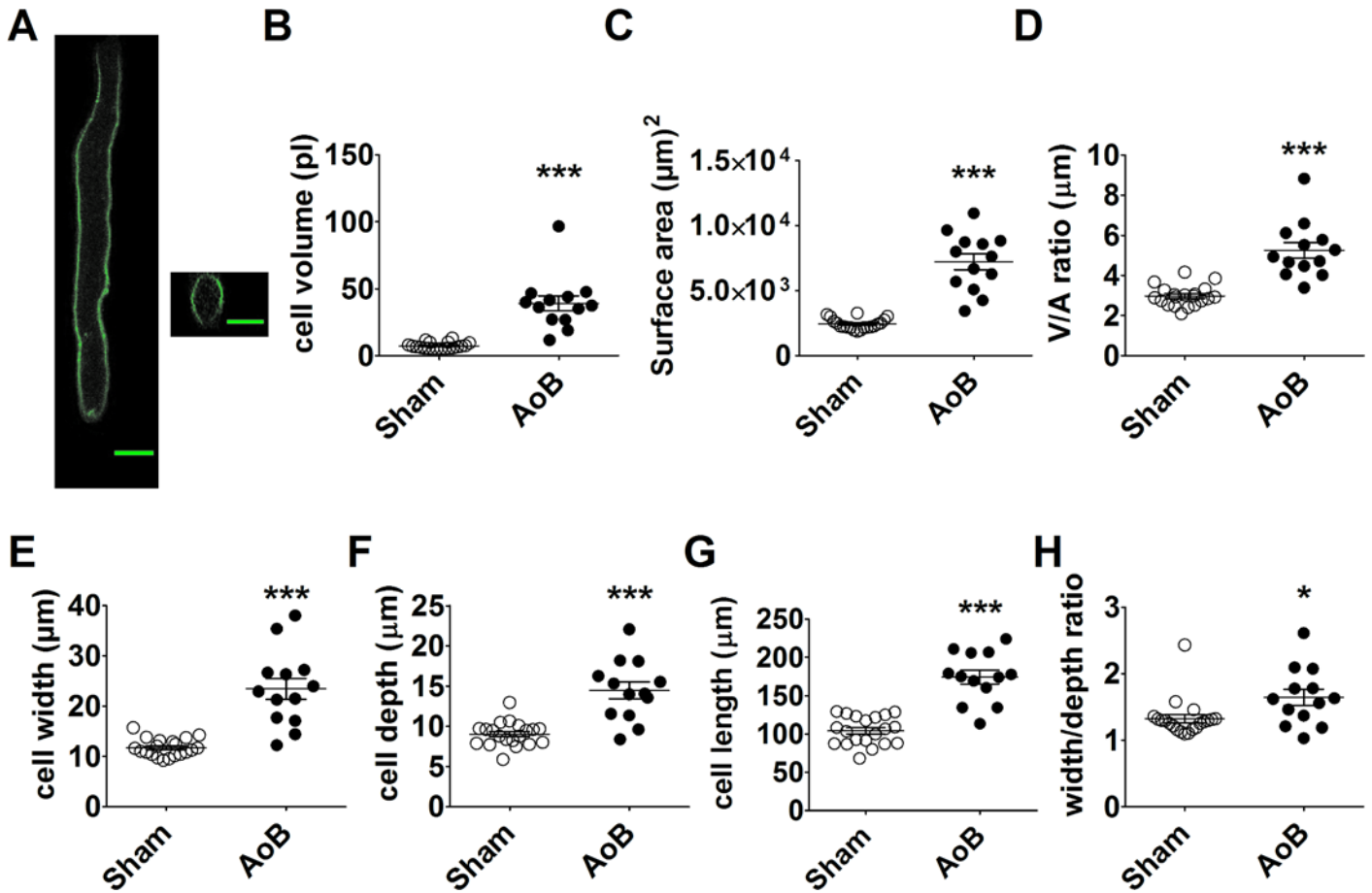
Fig 1. Left atrial myocyte hypertrophy. (A) left hand panel; total projected density of a series of x-y laser scanning images at various depths within an AoB left atrial myocyte stained with di-8-ANEPPS. Right hand panel; y-z section through the cell. Scale bar represents 20 μm. B–G respectively, cell volume (B), cell surface area (C), volume:surface area ratio (D), cell width (E), cell depth (F) and cell width:depth ratio of left atrial myocytes from Sham (open circles, n/N = 20/3) and AoB (filled circles, n/N = 13/3). Horizontal lines represent mean ± SEM. ###, P<0.0001, Student's unpaired t-test.

doi:10.1371/journal.pone.0144309.g001

by buffering equation:

$$J_B = k_{on}[Ca][B] - k_{off}[CaB]$$

Eq 6

ATP and fluo-3 were treated as mobile buffers and troponin as a fixed buffer (for constants see Table 1).

Ca uptake by the SR Ca²⁺ pump could be distributed across the cell volume:

$$J_{SERCA} = K_{max}\left(\frac{V_{max}}{1 + \left(K_m/[Ca^{2+}]\right)^2}\right) - J_{leak}$$

Eq 7

with K_m based on vesicle uptake experiments (1 μM[31]). An analogous equation was used to describe sarcolemmal Ca²⁺ extrusion with V_{max} being set to fit the observed time course of decline of the fluo-3 signal after a caffeine pulse. In the absence of an active SR pump the rate of Ca extrusion had to be increased by a factor of 170. J_{leak} is a constant to set net transport to zero for a resting [Ca²⁺] of 100 nM. Interpretation of local Ca²⁺ signals is further complicated by blurring due to the microscope point spread function, and this was simulated by convolving the model fluo-3 signal by 2D Gaussian function with full width at half maximum of 0.3 μm in

Table 1. Model diffusion and buffering constants.

Species	Concentration (μM)	Diffusion coefficient (10^{-10} m²/s)	k_{on} (μMs⁻¹)	k_{off} (s⁻¹)
Ca²⁺	0.1	3.0		
ATP(Ca)	0.2[a]	1.0	13.7 [b]	3.0×10^4
Mg²⁺	1000	0[a]	100	31
ATP(Mg)	495[a]	1.0	3.3×10^{-4}	3
Fluo-3	100	0.7	48.8	43.9
Troponin C	100	0	200	200

Table gives constants for the model which are based on previous cardiac simulation studies[29, 30] with minor adjustments in buffering parameters improve the fit to experimental data.

[a] The total ATP concentration was 5 mM, which was distributed among free, Ca²⁺ bound and Mg²⁺ bound forms according to equilibrium conditions.

[b] Diffusion of Mg²⁺ was ignored as tests showed that negligible gradients in Mg²⁺ developed.

doi:10.1371/journal.pone.0144309.t001

x,y and 1.0 μm in z, as estimated from images of fluorescent beads and in cells[29]. Calcium signals at the edge of the cells were produced by release basis function whose parameters were varied to fit experimental time courses:

$$J_{s,t} = R_{max}(\exp(-k_{off}t)(1 - \exp(-k_{on}t))) \qquad \text{Eq 8}$$

By solving the model reaction-diffusion equations and fitting results to experimental data, the requirement to deconvolve the fluorescent signals before trying to solve the inverse problem posed by the system of equations was overcome [29]. It should be noted that inverse solutions for the present problem would be (essentially) impossible due to experimental noise. Using this model we examined the spatio-temporal properties of Ca²⁺ transport across the cell to see whether Ca²⁺ signals in the center of the cell could be explained by purely passive diffusion or whether they required regenerative Ca²⁺ release.

Statistics

Data are expressed as mean ± standard error of the mean (SEM). Data sets were subject to D'Agostino and Pearson omnibus normality test. Statistical analyses applied are indicated in the figure legends. Sample sizes are reported as n/N, where n = number of cells and N = the number of hearts. $P < 0.05$ was considered statistically significant.

Results

Staining of the sarcolemma of isolated left atrial (LA) myocytes from both Sham and AoB rats with the lipophilic dye, di-8-ANEPPS, was located exclusively to the cell edge, consistent with a sparsity of t-tubules in these cells[32]. From confocal volume images the cell volume (Fig 1B), surface area (Fig 1C), volume/area ratio (Fig 1D), width (Fig 1E), depth (Fig 1F) and width/depth ratio (Fig 1G) were calculated. These data show that LA myocytes from AoB rats developed marked hypertrophy in comparison with cells from Sham controls.

The expression and phosphorylation of major proteins involved in Ca²⁺ transport was investigated by Western blotting of LA tissue homogenates from Sham and AoB rats (Fig 2). There were no significant differences between Sham and AoB in the expression of RyR2, SERCA, PLB or NCX1 (Fig 2B). On the other hand, expression of the α_{1c} subunit of LTCC was significantly reduced in AoB left atria as compared with Sham. There was no difference in the phosphorylation of RyR2 at the PKA/CaMKII sites, serine 2808 and serine 2814 or in the phosphorylation of PLB at serine 16.
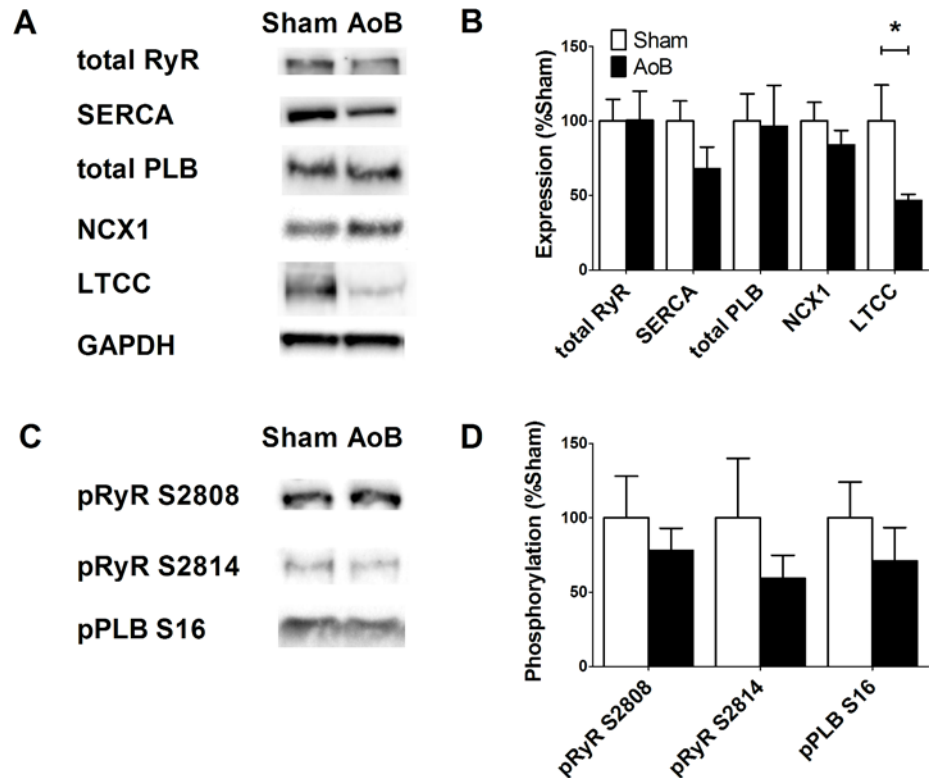
Fig 2. Left atrial expression of Ca^{2+} handling proteins. (A) Original Western blots of Ca^{2+} handling proteins from Sham and AoB LA. Note the GAPDH blots for normalization. (B) Mean band intensity expressed relative to Sham as 100%. Data represent mean ± SEM from 6 Sham and 6 AoB hearts. *, P<0.05, Student's unpaired *t*-test. (C) Original Western blots of phosphorylated RyR and PLB from Sham and AoB. Data correspond to the samples shown in (A). (D) Mean band intensity expressed relative to Sham as 100%. Data represent mean ± SEM from 6 Sham and 6 AoB hearts.

doi:10.1371/journal.pone.0144309.g002

Ryanodine receptor (RyR) labeling showed a clear striated pattern (Fig 3), as previously reported[17, 18, 33, 34]. However, there was no significant difference between Sham and AoB myocytes in the periodicity of staining of RyR2 at the sarcomeres (Sham: 0.550±0.005 μm^{-1}, $n = 18$; AoB: 0.552±0.004 μm^{-1}, $n = 18$; P = 0.71) or in the regularity of the staining associated with the striations (Sham: 6.0±0.8%; AoB: 4.7±0.6%; P = 0.19) as quantified by, respectively, the position and height of the peak from the Fourier transform. Western blot analysis confirmed no difference in RyR protein expression between Sham and AoB atria (Fig 2). The banded structure of the RyR labeling was consistent with the expression of RyR in corbular sarcoplasmic reticulum (SR) at the z-lines[17, 18, 33, 34]. RyR staining could be observed between the striations at the cell periphery in both Sham and AoB cells (white arrows in Fig 3A & 3B), consistent with the existence of RyR in junctional SR in close juxtaposition to the sarcolemma [17, 18, 33, 34]. Nevertheless, it is clear that the majority of RyR were not coupled to the sarcolemma. In summary, these data demonstrate that although left atrial myocytes from AoB rats had undergone significant afterload-induced hypertrophy, no remodeling of RyR expression or localization was evident.

Electrical stimulation of fluo-3-loaded cells elicited Ca^{2+}-transients that were initiated at the periphery of the cells (Fig 4). Ca^{2+}-transients at the edge of the cell were robust and rapidly reached a peak which was not different between the groups (F/F$_0$: Sham = 2.34±0.21, $n = 12$; AoB = 2.27±0.20, $n = 8$; P = 0.99). In contrast to the cell edge, transients at the center of the
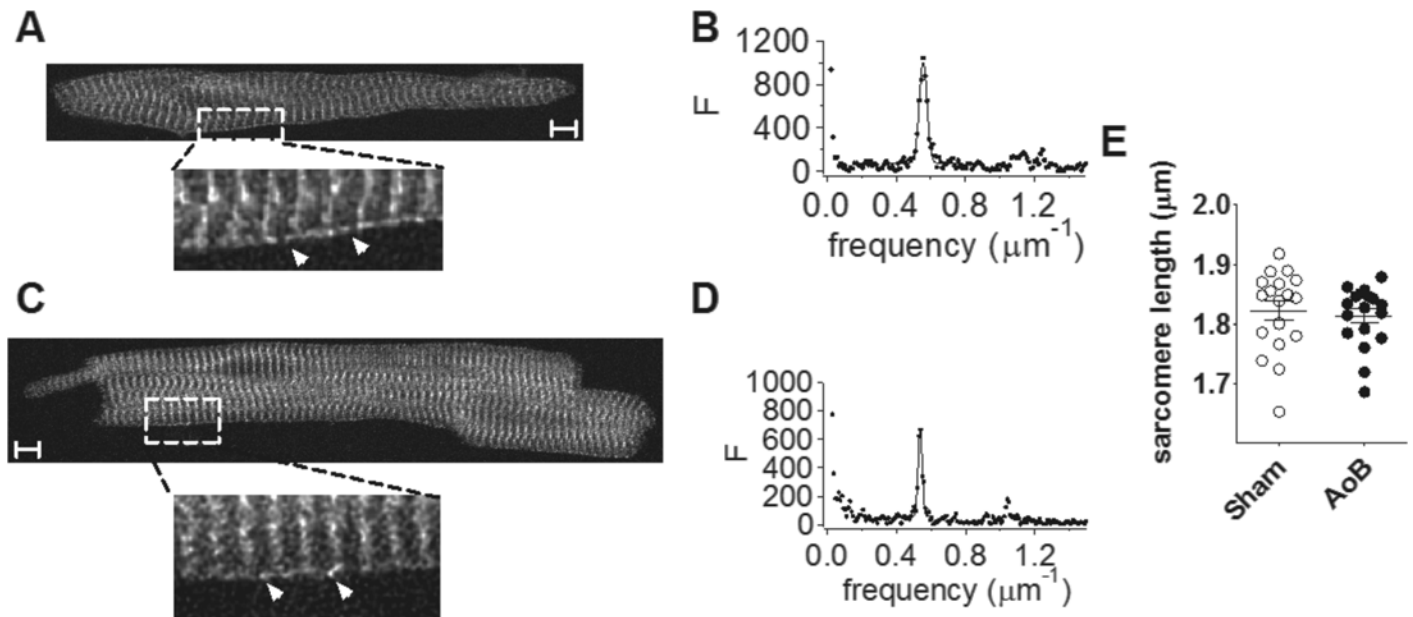
Fig 3. Ryanodine receptor location. (A) representative image from a Sham left atrial myocyte. Lower image, higher magnification view of area indicated by dotted box. Arrows indicate intra-sarcomeric RyR at the cell periphery. (B) power spectrum of longitudinal scan along the cell. (C) representative image from an AoB left atrial myocyte. Lower image, higher magnification view of area indicated by dotted box. (D) power spectrum of longitudinal scan along the cell. Scale bars represent 5 μm. (E) sarcomere length. Data from 18/3 Sham cells/hearts and 18/3 AoB cells/hearts.

cells had a much smaller amplitude (F/F_0: Sham = 1.22±0.04, P<0.0001; AoB = 1.28±0.09, P<0.0001) and were often barely detectable (e.g. Fig 4Ai & 4Bi). The delay to the center in these cells was Sham, 39.7±6.1 ms ($n = 10$), and AoB, 50.4±21.4 ms, ($n = 5$; P = 0.54). Thus, the cells generally showed a 'U'-shaped profile of Ca²⁺ changes across the width of the cell[35]. However, in a minority of cells (Sham 2/12; AoB 3/8; P = 0.35), significant transients could be observed at the cell center (e.g. Fig 4Aii & 4Bii). This variable pattern of release has previously been noted[36]. In summary, there were no significant differences between Sham and AoB myocytes in the amplitude of Ca²⁺ transients at the cell edge or at the cell center, nor was there any significant difference in the delay of the peak at the center of the cell relative to the cell edge.

The small amplitude of the Ca²⁺ transient at the cell center clearly suggests that in the majority of cells there was little, if any, regenerative propagation of Ca²⁺ release to the center. On the other hand, the short delay between the transient at the edge and center of the cell might be consistent with the propagation of a Ca²⁺ wave involving calcium-induced calcium release[37, 38]. These divergent possibilities led us to calculate the spatio-temporal time course of simple diffusion across an elliptical cell driven by a peripheral Ca²⁺ transient (see Methods and Fig 5A). A transient increase in [Ca²⁺]ᵢ to ~1 μM at the cell edge resulted in centripetal diffusion of Ca²⁺ and a significant Ca²⁺ transient occurred at the cell center (Fig 5B). However, the delay to the peak at the cell center relative to the peak of release at the cell edge (~100 ms) was considerably greater than that observed experimentally (*cf.* Fig 4). In addition, the amplitude of the transient at the cell center was greater than observed in the majority of cells. This difference between the model and experimental data could be explained by SR Ca²⁺ uptake across the cell, which, when added to the model equations, limited the effective spread of the transient to the cell center (Fig 5Ci) and reduced the time to peak and increased the rate of decline of the central Ca²⁺ transient. Adding simulated microscope blurring (measured from
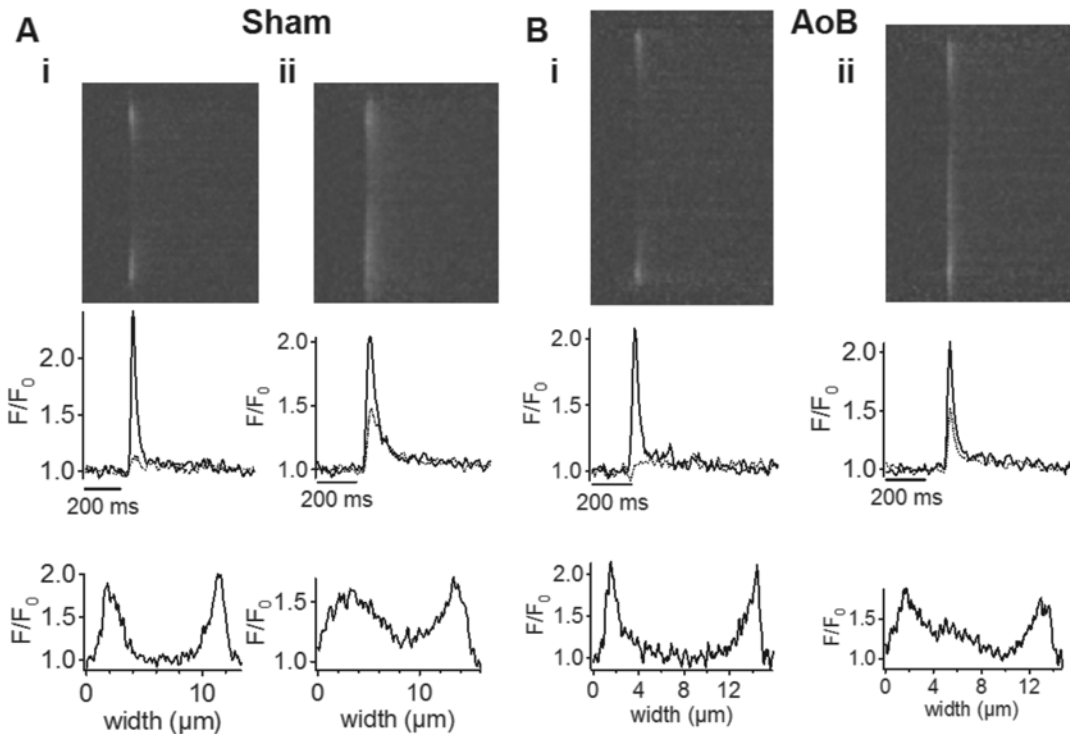
Fig 4. Left atrial myocyte Ca²⁺ transients in pressure-overload. (A) Upper panels: representative averaged line-scan images taken transversely across left atrial myocytes from Sham-operated rats. Middle panels: corresponding changes in $[Ca^{2+}]_i$ on the same time scale as the line-scan images. Black trace represents the signal at the edge of the cell, gray trace represents the signal in the center of the cell. Lower panels: transverse profile across the cell at the peak of the Ca²⁺ transient. (B) Upper panels: representative averaged line-scan images taken transversely across left atrial myocytes from AoB rats. Middle panels: corresponding changes in $[Ca^{2+}]_i$ on the same time scale as the line-scan images. Black trace represents the signal at the edge of the cell, gray trace represents the signal in the center of the cell. Lower panels: transverse profile across the cell at the peak of the Ca²⁺ transient. Cells were stimulated at 1 Hz.

fluorescent beads[29]) increased the apparent speed of propagation from the cell edge to center and resulted in model data being a reasonable facsimile of experimental data (compare Fig 5D and 5E with Fig 4). Thus, the data from most cells are consistent with the idea that Ca²⁺ release occurs predominately in cell periphery via junctional RyRs with little, if any, regenerative Ca²⁺ release from the uncoupled RyRs residing in corbular SR within the cell interior.

SR function was examined further using the RyR agonist, caffeine (Fig 6). Caffeine (10 mM) was applied 10 s after 8 conditioning pulses at 1 Hz. The application of caffeine produced a large homogeneous release of Ca²⁺ (Fig 6A), showing that the interior SR stored releasable Ca²⁺. After the peak of release, F/F_0 declined in the continued presence of caffeine, although more slowly than for twitch transients following electrical stimulation (Fig 6B). Following washout of caffeine, the amplitude of the Ca²⁺ transient was reduced, consistent with the loss of releasable Ca²⁺ from the junctional SR and with subsequent pulses Ca²⁺ release progressively increased in amplitude until a steady state was reached, typically after ~20 pulses. The amplitude of the caffeine-induced transient, an index of the Ca²⁺ content of the SR, was significantly smaller in AoB than in Sham myocytes (Fig 6C). This is consistent with a reduced expression of LTCC (and possibly SERCA) (Fig 2B) and a consequent decrease in Ca²⁺ influx and Ca²⁺ store uptake leading to reduced stored Ca²⁺. On the other hand, there was no notable difference between Sham and AoB myocytes in the recovery of Ca²⁺ transient amplitude following the washout of caffeine, suggesting that cytosolic Ca buffering was not increased in AoB myocytes

The contribution of different Ca²⁺ transporters to the extrusion of Ca²⁺ from the cytosol was examined by examining the rates of recovery of Ca²⁺ transients stimulated either
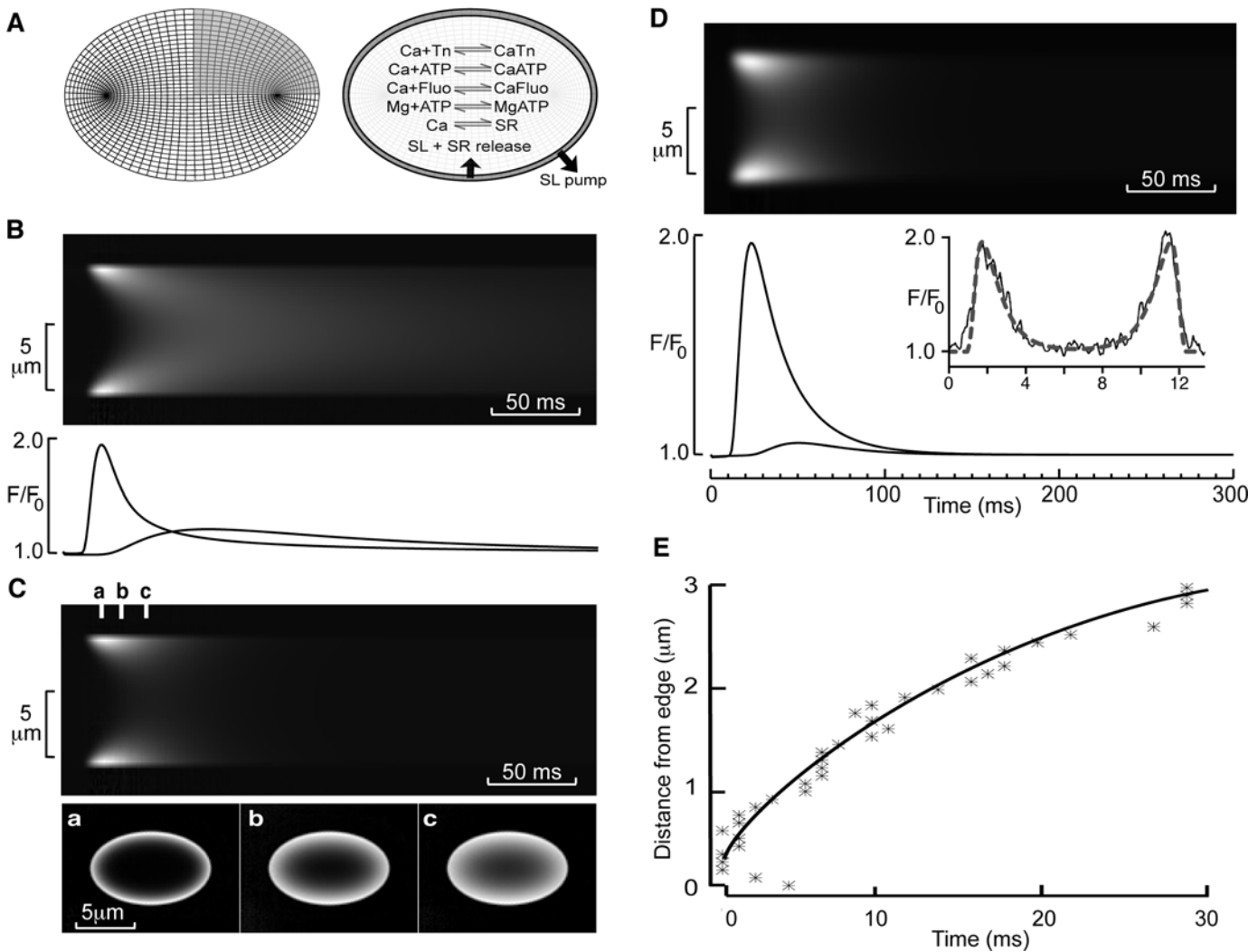
Fig 5. Modeling of diffusion in rat left atrial myocytes. (A) Model discretization with an elliptical grid and the Ca^{2+} reactions incorporated in the model representing Ca^{2+} buffering and fluxes. (B) Upper panel shows a simulated line scan image assuming release of Ca^{2+} only at the periphery of a cell and no *internal* Ca uptake. Lower panel shows relative fluorescence changes at the cell edge and cell center. Note the slow rate of decline of Ca^{2+} in the cell center. (C) Upper panel shows a simulated line scan image with SR Ca^{2+} uptake included. Lower panel shows the time course of fluorescence changes at the time points indicated by a, b and c in the upper panel. (D) Upper panel shows calculated line scan image including microscope blurring. Lower panel shows fluorescence changes at the edge and center of the cell model. The inset shows the radial profile at the peak of the transient for the model (dotted line) and exemplar experimental data (solid line). Note the close agreement between these data. (E) The time-dependence of spread of the peak fluorescence for the model (solid line) and exemplar experimental data (stars).

doi:10.1371/journal.pone.0144309.g005

electrically or by caffeine (Fig 7)[39, 40]. The rate of decline of electrically stimulated Ca^{2+} transients reflects extrusion via all pathways (i.e. the SR Ca^{2+} ATPase, NCX and sarcolemmal Ca^{2+} pump (SLCA)) (Fig 7A). In the presence of caffeine, the rate of recovery of the Ca^{2+} transient reflects sarcolemmal Ca^{2+} extrusion as the SR cannot accumulate Ca^{2+} (Fig 7B). In comparison with the electrically stimulated transient, the rate of decline of the Ca^{2+} transient in caffeine was reduced by about an order of magnitude and addition of 10 mM Ni^{2+} (to block NCX) further decreased the rate of decline of Ca^{2+} (Fig 7B) by a factor of ~3. There were no significant differences between Sham and AoB myocytes in the rate constants of Ca^{2+} extrusion during either twitch or caffeine-induced transients (Fig 7C) or in the presence of Ni^{2+} (Fig 7C), consistent with the absence of changes in expression of SERCA and NCX1 proteins (Fig 2). The
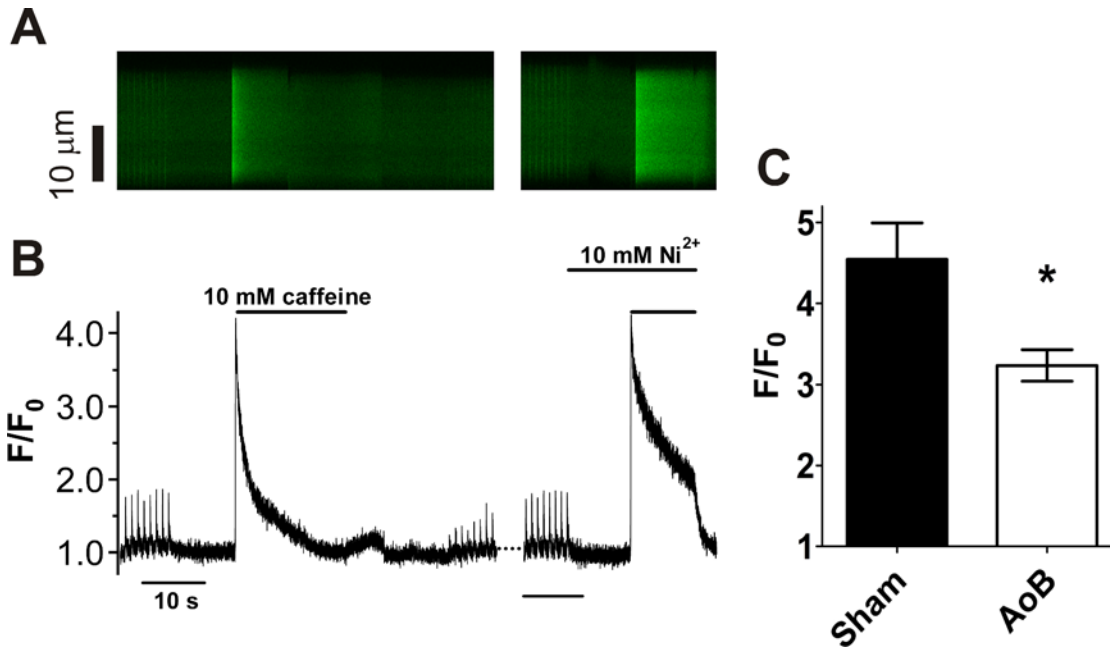
Fig 6. Caffeine-induced Ca²⁺ release. (A) representative line scan image of Ca²⁺ release triggered by caffeine (10 mM). Example is from a Sham myocyte. Time scale as shown in B. (B) time course of changes in spatially averaged $[Ca^{2+}]_i$ of the cell shown in A. Horizontal and vertical lines axes indicate $[Ca^{2+}]_i$ and time scale, respectively. (C) Mean (±SEM) peak F/F_0 in the presence of caffeine in Sham (n/N = 10/5) and AoB (n/N = 13/6) cells. *, P<0.05, unpaired t-test.

relative contribution of the transport pathways to Ca²⁺ extrusion were calculated from the rate constants[41] and no significant difference between Sham and AoB myocytes were found (Fig 7D).

In order to examine the impact of afterload-induced hypertrophic remodeling on susceptibility to spontaneous Ca²⁺ release, myocytes were subject to rapid pacing (Fig 8). Following rapid pacing, spontaneous Ca²⁺ transients occurred in both Sham and AoB myocytes (e.g. Fig 8A). The averaged profile of the spontaneous Ca²⁺ transients indicated that Ca²⁺ release was not confined to a particular location within the cell (Fig 8B). However, the proportion of cells showing spontaneous transients was significantly higher in AoB cells (92%) compared with Sham myocytes (50%; Fig 8C). In addition, the number of spontaneous transients observed per cell was greater in AoB cells than in Sham (Fig 8D).

Discussion

This study shows that increased afterload leads to atrial cell hypertrophy and an increased susceptibility to spontaneous Ca²⁺ transients. This mimics the reported increased atrial arrhythmia risk in hypertensive patients (e.g.[2]). In view of the central role of Ca²⁺ metabolism in the generation of spontaneous diastolic electrical activity[8], we examined Ca²⁺ transport and RyR distribution in the aortic banded model. Despite a large change in cell dimensions, Ca²⁺ transport and RyR distribution were hardly affected. There were no changes in the expression of RyR nor in RyR phosphorylation at the PKA/CaMKII sites, S2808 and S2814 (Fig 2) [21]. On the other hand, the amplitude of the caffeine-induced Ca²⁺ transient, an index of SR Ca²⁺ content, was reduced without any detectable change in transport via SERCA or NCX. Taken
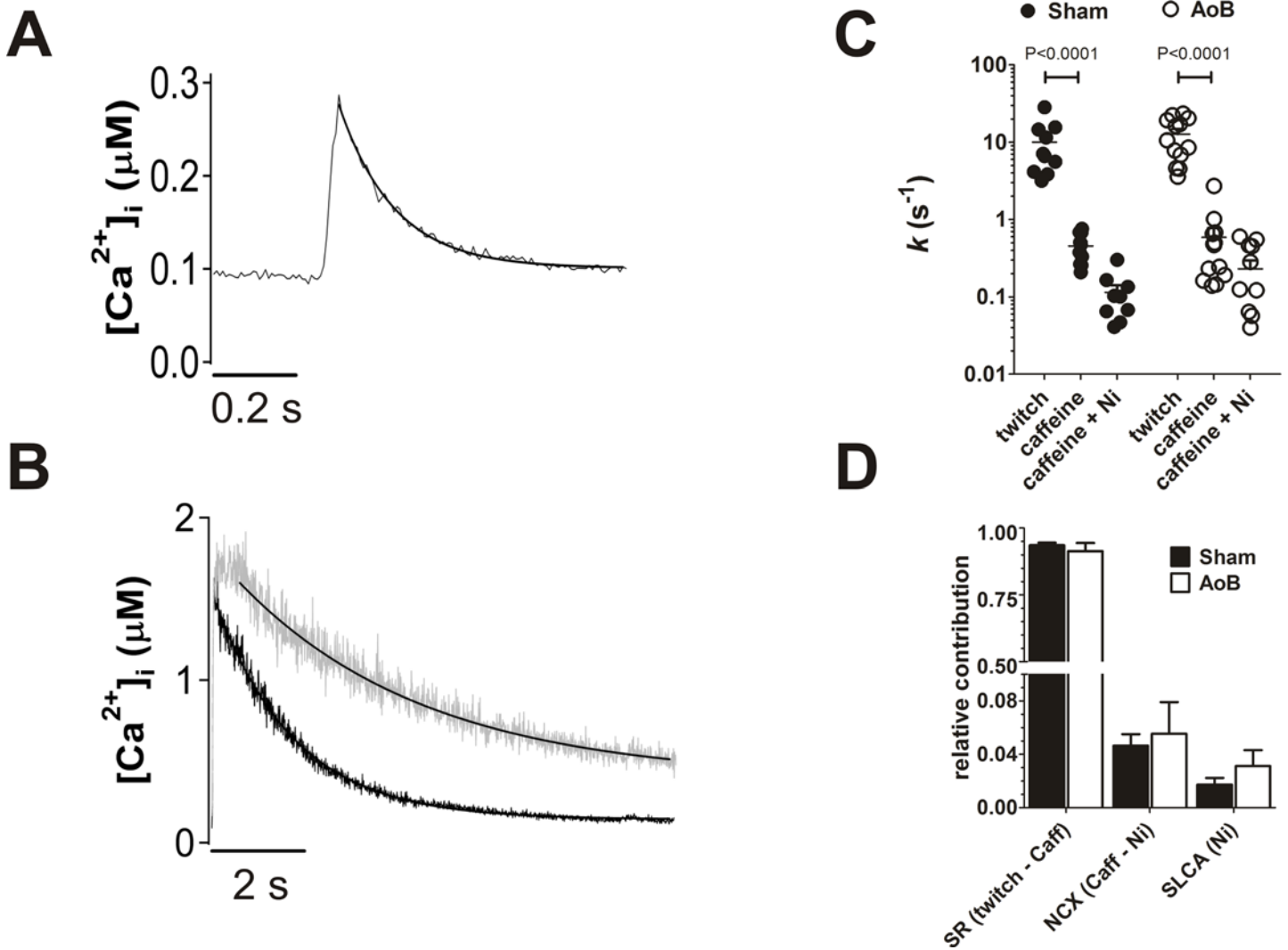
Fig 7. Ca^{2+} fluxes in hypertrophied atrial myocytes. (A) representative trace of twitch Ca^{2+} transient. The transient represents an average of 8 transients elicited prior to application of caffeine (see Fig 6). Solid line represents a fit to Eq 2. (B) representative traces of caffeine-induced Ca^{2+} transients in the absence (black trace) and presence (gray trace) of 10 mM Ni^{2+}. Solid lines represent fits to Eq 2. (C) fitted rate constants of Ca^{2+} removal from the cytosol in Sham (filled circles, n/N = 10/5) and AoB myocytes (open circles, n/N = 13/6). Horizontal bars represent means and vertical lines show standard errors. Data correspond with those shown in Fig 6C. (D) proportions of Ca^{2+} flux via the principal transport pathways calculated from the rate constants. There were no significant differences in rate constants or proportional fluxes between Sham and AoB.

together, our data are consistent with reduced LTCC expression, presumably resulting in decreased Ca^{2+} influx, in elevated afterload-induced atrial cellular remodeling.

Spatial heterogeneity in SR Ca^{2+} release

Myocytes exhibited marked non-uniformity in the Ca^{2+} transient across the width of the cell (e.g. lower panels of Fig 4Ai and 4Bi). By modeling 2D centripetal diffusion in an elliptical cell cross-section we showed that active SR Ca^{2+} uptake across the cell is essential to produce the spatio-temporal patterns of Ca^{2+} release observed. To our knowledge, this is the first report of such 2D modeling and shows that optical blurring by the microscope must also be considered to interpret correctly the spatio-temporal movements of Ca^{2+} across the cell width[29], and
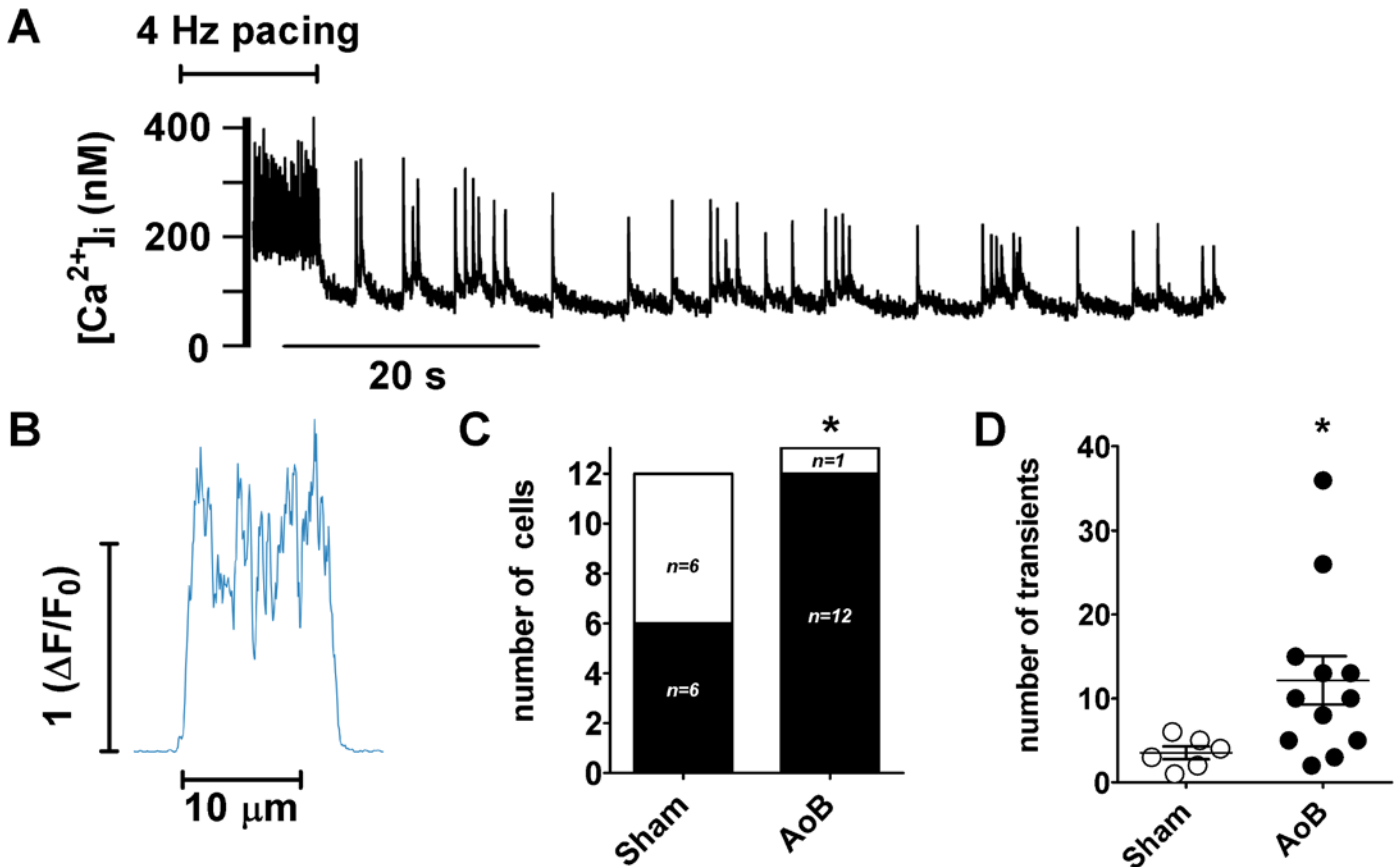
Fig 8. Spontaneous Ca²⁺ transients in remodeled left atrial myocytes. (A) Spatially averaged $[Ca^{2+}]_i$ obtained from an AoB cell during a period of pacing at 4 Hz followed by 70 s without stimulation. The resolution in these experiments was insufficient to localize the sites of release. (B) Averaged transverse profile of spontaneous Ca²⁺ transients from the cell shown in 'A'. (C) Shaded area indicates number of Sham and AoB myocytes showing spontaneous Ca²⁺ transients after 4 Hz pacing; height of column represents total number of myocytes tested. Data from 4 Sham and 6 AoB hearts. *, $P < 0.05$, Fischer's exact test. (D) Number of spontaneous transients in cells showing spontaneous activity after pacing at 4 Hz. *, $P < 0.05$, unpaired t-test.

doi:10.1371/journal.pone.0144309.g008

due to the cell ellipticity, reduction of the problem toward circular cylindrical models or even one dimension (as previously used in other studies) is likely erroneous.

The modeling shows that without SR Ca²⁺ uptake across the cell, the time course of decline of the internal Ca²⁺ transient is ~10 times slower (Fig 5B), showing that internal SR Ca²⁺ uptake plays a key role in making sure that the Ca²⁺ transient at the center of the cell is of comparable duration to that seen at the periphery. However, since little SR release occurs from the deeper SR (despite the presence of RyRs), the Ca²⁺ that is taken up must return to the cell surface by diffusion within the SR lumen (for subsequent release and/or extrusion), a process reminiscent of the SR vectorial transport and buffer barrier described for smooth muscle cells[42]. This will have been particularly significant following rapid pacing in the present study, when it can be expected that the SR would become loaded, particularly within the deeper SR, and this may contribute to the incidence of spontaneous Ca²⁺ release events in Sham cells (Fig 8) if the deep SR becomes overloaded (see also below).

Atrial Ca²⁺ regulation in hypertrophy

The present study is the first explicitly to examine Ca²⁺ regulation in a purely afterload-induced atrial hypertrophy. Spontaneous Ca²⁺ release has been reported to be increased in AF

in association with changes in RyR function, although SR Ca^{2+} content was reported to be unchanged and Na$^+$/Ca^{2+} exchange function increased[9–11, 43]. Reduced expression of the LTCC α_{1c} subunit has also been reported in human AF, associated with a decreased L-type Ca^{2+} current density [13, 15, 44]. Increased susceptibility to spontaneous Ca^{2+} release has been shown to lead to atrial arrhythmogenesis in a canine model of heart failure [23]. The increased susceptibility to spontaneous atrial Ca^{2+} release in heart failure has been associated with increased SR Ca^{2+} load despite reduced LTCC expression and Ca^{2+} current[23, 45, 46]. Our results contrast with those of a recent study of atrial cellular remodeling in a rat model of essential hypertension in which spontaneous Ca^{2+} release was *not* increased in atrial myocytes despite an increased SR Ca^{2+} load [47]. While, as found in the present study, LTCC expression was reduced, in contrast to our findings, expression of RyR2 and NCX1 was also reduced and phosphorylation of RyR2 at S2808 was increased[47]. In the present study, the amplitude of the electrically stimulated Ca^{2+} transient was not different between AoB and Sham myocytes, despite the reduced SR Ca^{2+} load and Ca^{2+} trigger via LTCC. That atrial effective refractory period has been reported to be unaffected in AoB hearts indicates that atrial action potential duration was unchanged[4]. Thus, these observations indicate that cytosolic buffering of Ca^{2+} was reduced in AoB cells, as has been recently reported in an ovine model of heart failure[46]. A reduction in cytosolic buffering would have diminished the difference between Sham and AoB cells in amplitude of the caffeine-induced transient. For example, in the absence of changes in SR Ca^{2+} load, a reduction in cytosolic buffering would have resulted in an *increase* in the amplitude of the caffeine-induced transient. Thus, the reduced amplitude of the caffeine-induced Ca^{2+} transient in AoB compared with Sham cells in the present study provides robust evidence of a reduction in atrial SR Ca^{2+} load through elevated afterload-induced remodeling.

The absence of differences in the present study between Sham and AoB in SERCA and NCX expression was reflected in the lack of difference in the rate constants of recovery of twitch and caffeine-induced Ca^{2+} transients, demonstrating that the activity of the major Ca^{2+} extrusion systems, the SR Ca^{2+} ATPase and the Na$^+$/Ca^{2+} exchanger, were not affected by the afterload-induced atrial hypertrophy. Moreover, the values of k_{twitch} and k_{Caff} were similar to those reported by Trafford and colleagues in normal atrial myocytes[28].

Given the key role played by SR luminal Ca^{2+} in regulating spontaneous release [48], it is notable that the increased susceptibility to spontaneous Ca^{2+} release in AoB compared with Sham atrial cells in the present study occurred despite reduced SR Ca^{2+} load. Presumably, the increased incidence of spontaneous release events in AoB cells reflects the increased volume of the cell: As there was no change in RyR distribution in the hypertrophied cells, the number of RyRs and potential release sites must have been increased across the cell (Fig 3), with the consequence that, even without a change in the RyR gating probability, the incidence of spontaneous release events following rapid pacing would be increased. Consistent with this proposal, the mean number of spontaneous transients per cell, including those cells that did not show spontaneous Ca^{2+} transients, was increased ~6.4-fold in AoB compared to Sham cells, a figure that corresponds well with the ~5.3-fold increased cell volume of AoB relative to Sham cells.

In summary, we have shown in an aortic banded model in rats that elevated afterload causes atrial cellular hypertrophy in which cellular Ca^{2+} transport and RyR2 distribution were unaffected but there was an increased susceptibility to spontaneous Ca^{2+} release, presumably reflecting maladaptive changes in cell geometry. We suggest that the increased susceptibility to spontaneous Ca^{2+} release reported here may underly the increased incidence of atrial tachyarrhythmias in conditions of elevated afterload.

Author Contributions

Conceived and designed the experiments: AFJ CHO. Performed the experiments: HZ SJK JJW RN. Analyzed the data: HZ JJW MBC AFJ. Contributed reagents/materials/analysis tools: SCC MBC. Wrote the paper: AFJ MBC.

References

1. Benjamin EJ, Chen P-S, Bild DE, Mascette AM, Albert CM, Alonso A, et al. Prevention of Atrial Fibrillation: Report From a National Heart, Lung, and Blood Institute Workshop. Circulation 2009; 119: 606–618. doi: 10.1161/CIRCULATIONAHA.108.825380 PMID: 19188521

2. Vagaonescu TD, Wilson AC, Kostis JB. Atrial Fibrillation and Isolated Systolic Hypertension: The Systolic Hypertension in the Elderly Program and Systolic Hypertension in the Elderly Program-Extension Study. Hypertension 2008; 51: 1552–1556. doi: 10.1161/HYPERTENSIONAHA.108.110775 PMID: 18391094

3. Choisy SCM, Arberry LA, Hancox JC, James AF. Increased Susceptibility to Atrial Tachyarrhythmia in Spontaneously Hypertensive Rat Hearts. Hypertension 2007; 49: 498–505. PMID: 17242301

4. Kim S-J, Choisy SCM, Barman P, Zhang H, Hancox JC, Jones SA, et al. Atrial Remodeling and the Substrate for Atrial Fibrillation in Rat Hearts with Elevated Afterload. Circ Arrhythm Electrophysiol 2011; 4: 761–769. doi: 10.1161/CIRCEP.111.964783 PMID: 21862733

5. Kistler PM, Sanders P, Dodic M, Spence SJ, Samuel CS, Zhao C, et al. Atrial electrical and structural abnormalities in an ovine model of chronic blood pressure elevation after prenatal corticosteroid exposure: implications for development of atrial fibrillation. Eur Heart J 2006; 27: 3045–3056. PMID: 17098760

6. Diness JG, Skibsbye L, Jespersen T, Bartels ED, Sørensen US, Hansen RS, et al. Effects on Atrial Fibrillation in Aged Hypertensive Rats by Ca²⁺-Activated K⁺ Channel Inhibition. Hypertension 2011; 57: 1129–1135. doi: 10.1161/HYPERTENSIONAHA.111.170613 PMID: 21502564

7. Lau DH, Shipp NJ, Kelly DJ, Thanigaimani S, Neo M, Kuklik P, et al. Atrial Arrhythmia in Ageing Spontaneously Hypertensive Rats: Unraveling the Substrate in Hypertension and Ageing. PLoS ONE 2013; 8: e72416. doi: 10.1371/journal.pone.0072416 PMID: 24013508

8. Wakili R, Voigt N, Kääb S, Dobrev D, Nattel S. Recent advances in the molecular pathophysiology of atrial fibrillation. J Clin Invest 2011; 121: 2955–2968. doi: 10.1172/JCI46315 PMID: 21804195

9. Hove-Madsen L, Llach A, Bayes-Genis A, Roura S, Font ER, Aris A, et al. Atrial Fibrillation Is Associated With Increased Spontaneous Calcium Release From the Sarcoplasmic Reticulum in Human Atrial Myocytes. Circulation 2004; 110: 1358–1363. PMID: 15313939

10. Neef S, Dybkova N, Sossalla S, Ort KR, Fluschnik N, Neumann K, et al. CaMKII-Dependent Diastolic SR Ca²⁺ Leak and Elevated Diastolic Ca²⁺ Levels in Right Atrial Myocardium of Patients With Atrial Fibrillation. Circ Res 2010; 106: 1134–1144. doi: 10.1161/CIRCRESAHA.109.203836 PMID: 20056922

11. Voigt N, Li N, Wang Q, Wang W, Trafford AW, Abu-Taha I, et al. Enhanced Sarcoplasmic Reticulum Ca²⁺-leak and Increased Na⁺-Ca²⁺-Exchanger Function Underlie Delayed Afterdepolarizations in Patients with Chronic Atrial Fibrillation. Circulation 2012; 125: 2059–2070. doi: 10.1161/CIRCULATIONAHA.111.067306 PMID: 22456474

12. Schotten U, Verheule S, Kirchhof P, Goette A. Pathophysiological Mechanisms of Atrial Fibrillation: A Translational Appraisal. Physiol Rev 2011; 91: 265–325. doi: 10.1152/physrev.00031.2009 PMID: 21248168

13. Workman AJ, Kane KA, Rankin AC. The contribution of ionic currents to changes in refractoriness of human atrial myocytes associated with chronic atrial fibrillation. Cardiovasc Res 2001; 52: 226–235. PMID: 11684070

14. Christ T, Boknik P, Wohrl S, Wettwer E, Graf EM, Bosch RF, et al. L-Type Ca²⁺ Current Downregulation in Chronic Human Atrial Fibrillation Is Associated With Increased Activity of Protein Phosphatases. Circulation 2004; 110: 2651–2657. PMID: 15492323

15. Bosch RF, Zeng X, Grammer JB, Popovic K, Mewis C, Kühlkamp V. Ionic mechanisms of electrical remodeling in human atrial fibrillation. Cardiovasc Res 1999; 44: 121–131. PMID: 10615396

16. Berlin JR, Cannell MB, Lederer WJ. Cellular origins of the transient inward current in cardiac myocytes. Role of fluctuations and waves of elevated intracellular calcium. Circ Res 1989; 65: 115–126. PMID: 2736729

17. Chen-Izu Y, McCulle SL, Ward CW, Soeller C, Allen BM, Rabang C, et al. Three-Dimensional Distribution of Ryanodine Receptor Clusters in Cardiac Myocytes. Biophys J 2006; 91: 1–13. PMID: 16603500

18. Kockskamper J, Sheehan KA, Bare DJ, Lipsius SL, Mignery GA, Blatter LA. Activation and Propagation of Ca^{2+} Release during Excitation-Contraction Coupling in Atrial Myocytes. Biophys J 2001; 81: 2590–2605. PMID: 11606273

19. Isenberg G, Klockner U. Calcium tolerant ventricular myocytes prepared by preincubation in a "KB medium". Pflugers Archiv 1982; 395: 6–18. PMID: 7177773

20. Brette F, Komukai K, Orchard CH. Validation of formamide as a detubulation agent in isolated rat cardiac cells. Am J Physiol 2002; 283: H1720–H1728.

21. Stange M, Xu L, Balshaw D, Yamaguchi N, Meissner G. Characterization of Recombinant Skeletal Muscle (Ser-2843) and Cardiac Muscle (Ser-2809) Ryanodine Receptor Phosphorylation Mutants. J Biol Chem 2003; 278: 51693–51702. PMID: 14532276

22. Vest JA, Wehrens XHT, Reiken SR, Lehnart SE, Dobrev D, Chandra P, et al. Defective Cardiac Ryanodine Receptor Regulation During Atrial Fibrillation. Circulation 2005; 111: 2025–2032. PMID: 15851612

23. Yeh Y-H, Wakili R, Qi X-Y, Chartier D, Boknik P, Kääb S, et al. Calcium-Handling Abnormalities Underlying Atrial Arrhythmogenesis and Contractile Dysfunction in Dogs With Congestive Heart Failure / CLINICAL PERSPECTIVE. Circ Arrhythm Electrophysiol 2008; 1: 93–102. doi: 10.1161/CIRCEP.107.754788 PMID: 19808399

24. Shan J, Kushnir A, Betzenhauser MJ, Reiken S, Li J, Lehnart SE, et al. Phosphorylation of the ryanodine receptor mediates the cardiac fight or flight response in mice. J Clin Invest 2010; 120: 4388–4398. doi: 10.1172/JCI32726 PMID: 21099118

25. van Oort RJ, McCauley MD, Dixit SS, Pereira L, Yang Y, Respress JL, et al. Ryanodine Receptor Phosphorylation by Calcium/Calmodulin-Dependent Protein Kinase II Promotes Life-Threatening Ventricular Arrhythmias in Mice With Heart Failure / Clinical Perspective. Circulation 2010; 122: 2669–2679. doi: 10.1161/CIRCULATIONAHA.110.982298 PMID: 21098440

26. Fischer TH, Herting J, Tirilomis T, Renner A, Neef S, Toischer K, et al. Ca^{2+}/Calmodulin-Dependent Protein Kinase II and Protein Kinase A Differentially Regulate Sarcoplasmic Reticulum Ca^{2+} Leak in Human Cardiac Pathology. Circulation 2013; 128: 970–981. doi: 10.1161/CIRCULATIONAHA.113.001746 PMID: 23877259

27. Cannell MB, Cheng H, Lederer WJ. Spatial non-uniformities in [Ca^{2+}]$_i$ during excitation-contraction coupling in cardiac myocytes. Biophys J 1994; 67: 1942–1956. PMID: 7858131

28. Walden AP, Dibb KM, Trafford AW. Differences in intracellular calcium homeostasis between atrial and ventricular myocytes. J Mol Cell Cardiol 2009; 46: 463–473. doi: 10.1016/j.yjmcc.2008.11.003 PMID: 19059414

29. Kong CHT, Laver DR, Cannell MB. Extraction of Sub-microscopic Ca Fluxes from Blurred and Noisy Fluorescent Indicator Images with a Detailed Model Fitting Approach. PLoS Comput Biol 2013; 9: e1002931. doi: 10.1371/journal.pcbi.1002931 PMID: 23468614

30. Soeller C, Cannell MB. Numerical simulation of local calcium movements during L-type calcium channel gating in the cardiac diad. Biophys J 1997; 73: 97–111. PMID: 9199775

31. Berrebi-Bertrand I, Lahouratate P, Lahouratate V, Camelin JC, Guibert J, Bril A. Mechanism of Action of Sarcoplasmic Reticulum Calcium-Uptake Activators. Eur J Biochem 1997; 247: 801–809. PMID: 9288900

32. Yamasaki Y, Furuya Y, Araki K, Matsuura K, Kobayashi M, Ogata T. Ultra-high-resolution scanning electron microscopy of the sarcoplasmic reticulum of the rat atrial myocardial cells. Anat Rec 1997; 248: 70–75. PMID: 9143669

33. Carl SL, Felix K, Caswell AH, Brandt NR, Ball WJ Jr, Vaghy PL, et al. Immunolocalization of sarcolemmal dihydropyridine receptor and sarcoplasmic reticular triadin and ryanodine receptor in rabbit ventricle and atrium. J Cell Biol 1995; 129: 672–682.

34. Mackenzie L, Bootman MD, Berridge MJ, Lipp P. Predetermined recruitment of calcium release sites underlies excitation-contraction coupling in rat atrial myocytes. J Physiol (Lond) 2001; 530: 417–429.

35. Kirk MM, Izu LT, Chen-Izu Y, McCulle SL, Wier WG, Balke CW, et al. Role of the transverse-axial tubule system in generating calcium sparks and calcium transients in rat atrial myocytes. J Physiol (Lond) 2003; 547: 441–451.

36. Woo S-H, Cleemann L, Morad M. Diversity of atrial local Ca^{2+} signalling: evidence from 2-D confocal imaging in Ca^{2+}-buffered rat atrial myocytes. J Physiol (Lond) 2005; 567: 905–921.

37. Takamatsu T, Gil Weir W. Calcium waves in mammalian heart: quantification of origin, magnitude, waveform and velocity. FASEB J 1990; 4: 1519–1525. PMID: 2307330

38. O'Neill SC, Miller L, Hinch R, Eisner DA. Interplay between SERCA and sarcolemmal Ca^{2+} efflux pathways controls spontaneous release of Ca^{2+} from the sarcoplasmic reticulum in rat ventricular myocytes. J Physiol (Lond) 2004; 559: 121–128.

39.   Negretti N, O'Neill SC, Eisner DA. The relative contributions of different intracellular and sarcolemmal systems to relaxation in rat ventricular myocytes. Cardiovasc Res 1993; 27: 1826–1830 PMID: 8275530

40.   Bassani JWM, Bassani RA, Bers DM. Relaxation in rabbit and rat cardiac cells: species dependent differences in cellular mechanisms. J Physiol (Lond) 1994; 476: 279–293.

41.   Dibb KM, Rueckschloss U, Eisner DA, Isenberg G, Trafford AW. Mechanisms underlying enhanced cardiac excitation contraction coupling observed in the senescent sheep myocardium. J Mol Cell Cardiol 2004; 37: 1171–1181. PMID: 15572047

42.   Chen Q, Cannell M, van Breemen C. The superficial buffer barrier in vascular smooth muscle. Can J Physiol Pharmacol 1992; 70: 509–514. PMID: 1386774

43.   Lenaerts I, Bito V, Heinzel FR, Driesen RB, Holemans P, D'Hooge J, et al. Ultrastructural and Functional Remodeling of the Coupling Between Ca^{2+} Influx and Sarcoplasmic Reticulum Ca^{2+} Release in Right Atrial Myocytes From Experimental Persistent Atrial Fibrillation. Circ Res 2009; 105: 876–885. doi: 10.1161/CIRCRESAHA.109.206276 PMID: 19762679

44.   Grammer JB, Zeng X, Bosch RF, Kuhlkamp V. Atrial L-type Ca^{2+}-channel, β-adrenoreceptor, and 5-hydroxytryptamine type 4 receptor mRNAs in human atrial fibrillation. Basic Res Cardiol 2001; 96: 82–90. PMID: 11215536

45.   Li D, Melnyk P, Feng J, Wang Z, Petrecca K, Shrier A, et al. Effects of Experimental Heart Failure on Atrial Cellular and Ionic Electrophysiology. Circulation 2000; 101: 2631–2638. PMID: 10840016

46.   Clarke JD, Caldwell JL, Horn MA, Bode EF, Richards MA, Hall MCS, et al. Perturbed atrial calcium handling in an ovine model of heart failure: Potential roles for reductions in the L-type calcium current. J Mol Cell Cardiol 2015; 79: 169–179. doi: 10.1016/j.yjmcc.2014.11.017 PMID: 25463272

47.   Pluteanu F, Heß J, Plackic J, Nikonova Y, Preisenberger J, Bukowska A, et al. Early subcellular Ca^{2+} remodeling and increased propensity for Ca^{2+} alternans in left atrial myocytes from hypertensive rats. Cardiovasc Res 2015; 106: 87–97. doi: 10.1093/cvr/cvv045 PMID: 25691541

48.   Zima AV, Bovo E, Bers DM, Blatter LA. Ca^{2+} spark-dependent and -independent sarcoplasmic reticulum Ca^{2+} leak in normal and failing rabbit ventricular myocytes. J Physiol (Lond) 2010; 588: 4743–4757.